Imperial College London

Department of AERONAUTICS

Ammonia-Powered Regional Aircraft

Lift distribution Optimization and Fairing Design

Group Design Project - Individual Report

APR03: Aerodynamics

Project Lead: Dr. Rob Hewson
Academic Supervisor: Burhan Saeed
Department: Department of Aeronautics
Course: MEng Aeronautical Engineering
Module: AERO60004 Group Design Project
Academic Year: 2022/23

Student: Edward Grantham
CID: 01848149
GDP Group: 04
Date June 19, 2023

Department of Aeronautics
South Kensington Campus
Imperial College London
London SW7 2AZ
U.K.

Abstract

The aim of this project was to design an ammonia powered regional aircraft as a lower environmental impact alternative to similar aircraft. This report focused on the optimization of this aircraft's span-wise lift distribution as well as the design and drag analysis of a wing fuselage fairing. The lift distribution optimization consisted of using geometric twist to enforce as close to an elliptical lift distribution as possible. This was completed on a higher accuracy model of lift distribution achieved using the collocation method of the lifting line theory. This method was also used to incorporate the effect of the fuselage and propeller/nacelle wing interaction. This optimization yielded a decrease in induced drag from 137.2% to 117.5% of the minimum possible elliptical lift distribution induced drag. The design of a wing fuselage fairing consisted of using a standard shape from literature shown to reduce interference factor. The fairing shape was then sized according to literature, a CFD report and this design's specific dimensions before being smoothly incorporated into other geometries. This design lead to a potential decrease in drag of $\Delta C_{D_{fair}}$=0.0018. The extra zero lift drag caused by the shape of the fairing and its interaction with the boundary layer was also calculated to be $C_{D_{0,fair}}$=0.00168. As the zero lift drag caused by the fairing was less than the decrease in drag caused by the fairing, it was decided to implement the fairing. However due to the closeness of the drag values, further analysis was concluded to be required.

Sub-Teams Breakdown

Sub-Team	Name
APR01: Configuration Definition	Ahmad Shahizam, Zayd Kashyap, Aaditya Liu, Bella Ng, Paul
APR02: Propulsion Systems	El Khatib, Maram Lee, Andrew Mackie, Joseph Moussa, Ahmed Shi, Lidan
APR03: Aerodynamics	Alsree, Hafiz Alsree Grantham, Edward Kulacz, Luca Liu, Mingpu Sharma, Tej
APR04: Structural Design and Manufacturing	Ariyaratnam, Shapeetha Popa, Erminia Riddell, Alfred Sun, Haoyuan Yan, Qiutong
APR05: Flight Dynamics and Control	Liu, Kee Kwan Obasa, Remi Vegad, Kapil Weng, Cenhao Zhang, Jacky
APR06: Aircraft Ground Infrastructure, Energy Storage and Overall Operating Costs	Goh, Wen Xu Samuel, Amelia See, Joseph

Contents

List of Figures

List of Tables

Nomenclature

A_n	Fourier Coefficients
a	Lift curve slope
AR	Aspect Ratio
c	Chord
C_D	Drag coefficient
$(C_D)_{\delta=0}$	Zero incidence profile drag
C_l	Lift coefficient
C_T	Thrust Coefficient coefficient
e	Oswald efficiency factor
h/δ	Ratio of fairing height to boundary layer thickness
I_s	Smoothing Index
i_w	Incidence angle
L	Lift
M	Mach number
m	Boundary layer power law index
q	Dynamic pressure
S	Area
s	Wing span
T	Thrust
U_∞	Free stream velocity
v	Velocity
W_t	Propeller wash tangential velocity
W_t	Propeller wash axial velocity
α	Angle of attack
α_0	Zero lift angle of attack
$(1+\delta)$	Wing span-wie efficiency factor
ϵ	Twist angle
Γ	Circulation
λ	Taper Ratio
Λ_{25}	Quarter Chord Sweep
ρ	Density

1 Introduction

The purpose of this project was to design a regional aircraft which uses ammonia as its fuel in order to reduce its environmental impact. This novel design imposed the following design objectives on the aerodynamics team. Firstly integrate the required ammonia fuel and propulsion systems in a safe and aerodynamically optimal manner. Secondly, reduce the aircraft's overall drag therefore reducing the thrust requirement required of the novel propulsion system.

This report mainly focuses on the optimization of the aircraft's lift distribution. This was done by varying geometric twist in order to enforce as close to an elliptical distribution as possible while accounting for affects caused by the fuselage as well as the propeller/nacelle on the wing. This report also details the design and drag analysis of a wing fuselage fairing in order to further reduce drag.

2 Lift Distribution Optimization

2.1 Initial Planform

The first approximation of an elliptical lift distribution was derived from an empirical method from literature which involved selecting a constant taper ratio to best approximate an elliptical distribution. The optimal taper ratio is a function of a wing's sweep and twist, and is given by equation 1 [1]. This yielded an initial estimate of 0.450 as sweep was previously determined to be 0 degrees. This value however does not account for twist which was previously specified for stability reasons. To account for this an empirical fudge factor of 1.18 [2] yields an initial taper ratio of 0.531. This method was used as a quick approximation to give an estimate of wing parameters such that other analysis could be done.

$$\lambda = 0.45e^{-0.036\Lambda_{25}} \tag{1}$$

2.2 Collocation Script

While the previous methods provide a reasonable taper ratio to approximate an elliptical distribution, it does not give insight on the actual shape of the distribution. To better model a wings lift distribution, the collocation method of the lifting line theory was explored. This method involves discretizing a wing into a number of collocation points (at angles θ) at which circulation and therefore lift are modelled as a Fourier series as given by equation 2 [3].

$$\Gamma(\theta) = 4sU_\infty \sum_{n=1}^{\infty} A_n sin(n\theta) \tag{2}$$

$$L = 4\rho U_\infty^2 s^2 A_1 \frac{\pi}{2} \tag{3}$$

The first Fourier coefficient is a function of the lift produced as given by equation 3 while the following Fourier coefficients are solved as a set of simultaneous equations. The equations for which are given by an alternative form of equation 2 shown in equation 4, solved at the number of collocation points chosen . This means that generally a higher number of collocation increases the accuracy of the lift distribution shape. Increasing the number of collocation points too high however results in ill conditioning. This results in the results being very sensitive to small changes in the Fourier coefficients to a point where numerical accuracy (float point error) can worsen the accuracy. This problem is further exacerbated when optimizing the lift distribution as explored later. This lead to the choice of 20 panels which was found to be sufficient to smoothly model lift distributions and calculate induced drag accurately to three decimal places.

$$\sum_{n=1}^{\infty} A_n sin(n\theta)(n\mu + sin\theta) = \mu\alpha sin(\theta) \tag{4}$$

$$\mu = \frac{a_0 c}{8s} \tag{5}$$

As well as providing a more accurate lift distribution shape, the collocation method also gives a more accurate estimate of induced drag as given by equations 6 and 7. The variable $(1+\delta)$ known as the wing span-wise efficiency factor accounts for the extra induced drag caused by a non-elliptical lift distribution by summing all Fourier coefficients after the first according to equation 7 . For an elliptical distribution, all Fourier coefficients after the first equal zero giving a span-wise efficiency factor of 1 therefore minimum possible induced drag. The main aim of this report is to enforce the design's lift distribution to be as close to elliptical as possible therefore reducing induced drag.

$$C_{D_i} = \frac{C_l^2(1+\delta)}{\pi AR} \tag{6}$$

$$\delta = \sum_{n=2}^{\infty} nA_n^2, \tag{7}$$

2.3 Refined Constant Taper

This script was initially used to revise the taper ratio . This was done by calculating the root mean square error between all taper ratios and an eliptical lift distribution as can be seen in fig.1. From this a more optimal taper ratio of 0.79 was selected. Fig. 2 shows the difference in lift distribution with the different taper ratios where 0.79 can be seen to be closer to the desired elliptical distribution than 0.531. This is also reflected by a 56.5% difference in root mean square between the two taper ratios. Due to an internal deadline on fixing all wing planform parameters in order to complete other sizing, the optimal taper ratio changed from the selected 0.79 to 0.77 due to small changes in weight. This however only changes root mean square error by 1% and it was decided to keep the current taper ratio of 0.79 as the disruptive affect of changing the planform outweighs the small improvement in efficiency.

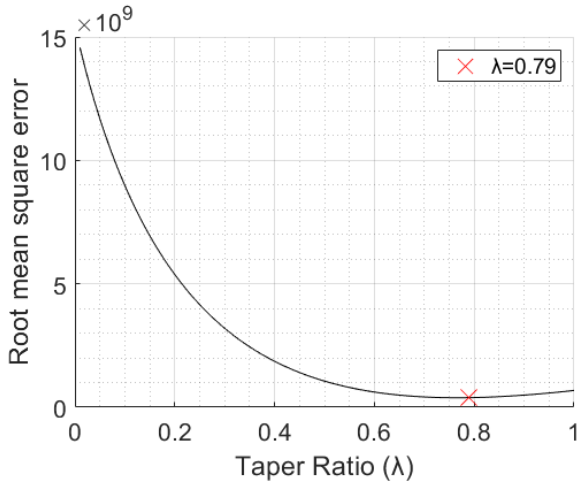

Figure 1: Root mean square error of span-wise lift distribution at different taper ratios

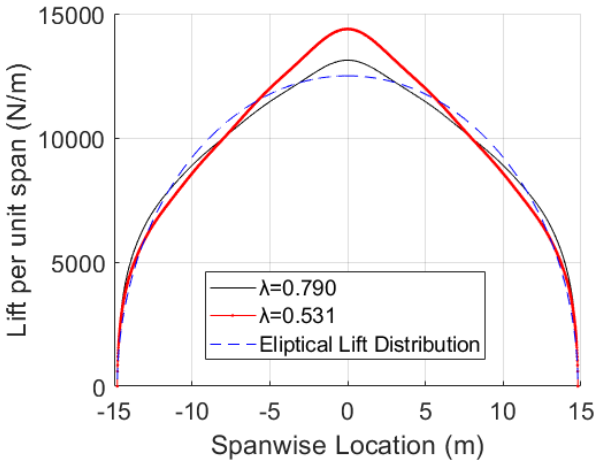

Figure 2: Lift distribution at taper ratios of 0.790 and 0.531

2.4 Optimization Variable Selection

As previously seen, lift at a position is a function of the chord (c) and local angle of attack (α). Local angle of attack is a function of zero lift angle of attack (α_0) and twist angle (ϵ). The lift distribution can therefore be altered by either varying wing taper, geometric or aerodynamic twist. To thoroughly optimize the lift distribution, one of the variables will likely have to be varied in a non-linear manner which presents practical problems.

Varying wing taper non-linearly would likely be highly complex and costly for manufacturing reasons. Varying taper also requires the spars to be closer together to provide reasonable margin for chord changes. This is especially constraining due to the novel safety issues of ammonia which lead

to the decision to house all the fuel within the wing . Varying taper would therefore either reduce the volume available for fuel or limits the ability to enforce an elliptical lift distribution using taper. A constant taper ratio of 0.79 was therefore chosen as it is the closest to elliptical, reducing adjustments needed to be made by other variables. Both aerodynamic and geometric twist would not impose the same constraints on the wing in terms of fuel storage or manufacturing as both twists are enforced with small changes to rib cross sections.

Modern commercial aircraft typically use a combination of both geometric and aerodynamic twist to enforce the desired lift distribution [4] . It was however chosen to just optimize using one variable for simplicity as there are infinite combination when optimizing with multiple variables. One variable also proved to be sufficient to enforce the desired lift distribution, therefore not requiring additional twist from the other method. To optimize using aerodynamic twist would involve linearly interpolating between root and tip aerofoils with many intermediary aerofoils. The exact aerodynamic properties of those intermediary aerofoils would be unknown without experimental results. In contrast using geometric twist simply changes the local angle of attack for the same aerofoil for which there is higher confidence in its behaviour. So many non-linearly changing aerofoils would also make control analysis more complex. Geometric twist was therefore chosen to optimize for the desired lift distribution.

2.5 Initial Twist optimization

The collocation method script developed was used to optimize twist to an elliptical lift distribution. This was done by solving for the required local angle of attack needed at all collocation points using equation 4 to fit the elliptical distribution. From this value, the twist angle (ϵ) was found using equation 8 with zero lift angle of attack being known and incidence angle sized to meet the required lift.

$$\alpha = \epsilon + \alpha_0 - i_w \tag{8}$$

This methodology yielded the lift distribution in fig.3. This shows that the collocation method is able to enforce a elliptical lift distribution very well as it is able to give a perfect span-wise efficiency factor to three decimal places ($(1+\delta)$=1.000). The twist distribution needed to achieve this seen in fig.4 is also reasonable as it requires reasonable magnitude twist to enforce the desired distribution meaning additional aerodynamic twist is not required. The sharp change at the wing tips is due to a -3°twist angle being prescribed for stability reasons.

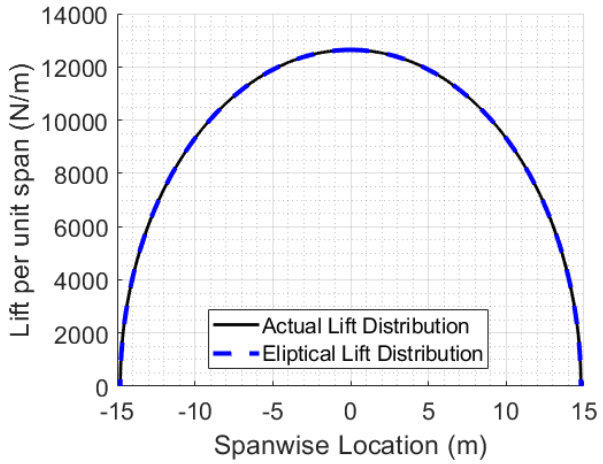

Figure 3: Initial Twist optimized lift distribution compared with an elliptical distribution.

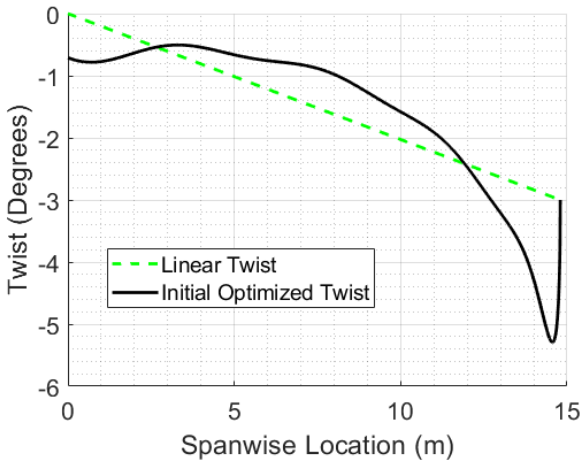

Figure 4: Twist distribution needed to enforce a elliptical distribution

2.6 Propeller Wash/Nacelle Wing Interaction

The previous methodologies have assumed that the the wing is clean and entirely uninterrupted ,this however is not the case. Many variables other than those included in the collocation method can affect the lift distribution. The two factors which most affect lift distribution on this configuration is the propeller wash/nacelle-wing interaction and the fuselage-wing interaction.

This aircraft's propulsion system was chosen to be a turbo prop due to the low cruise speed of 0.45 mach as well as benefits related to the novel ammonia fuel system. The location of the nacelle was determined as wing mounted due to the desire to attach the undercarriage to it. A pusher configuration was chosen such that the propeller does not need to operate in turbulent air [5]. This poses two elements that will affect the wings lift distribution, namely a wing mounted nacelle and the velocity induced by the propeller (known as the propeller wash) over the nacelle and wing.

As the dimensions of the nacelle are such that they fit entirely within the prop wash, these two phenomena are difficult to separate. It was therefore chosen to source data from a CFD study [6] of the combined affect of both on a wings lift distribution.

The affect of propeller wash on a wing is made of two primary phenomena. The first is an increase in lift caused by the higher propeller wash velocity the wing sees according to equation 9. This increased lift then results in a higher lift coefficient over the affected area when taken with reference to the same free stream velocity as unaffected regions.

$$L = \frac{1}{2} C_L \rho v^2 S \tag{9}$$

The 2nd phenomena is caused by the rotational velocity induced in the propeller wash. This rotational velocity known as swirl is a result of the torque applied to the propeller in order for it to produce thrust [7]. This rotational velocity results in a positive tangential component of the propeller wash velocity (W_t) on the side of the propeller for which the blade is on the upswing. This results in an increased effective angle of attack as seen in fig.5 [8], therefore lift coefficient on that side. On the other side there is a downwards velocity component causing a decrease in angle of attack and therefore lift coefficient.

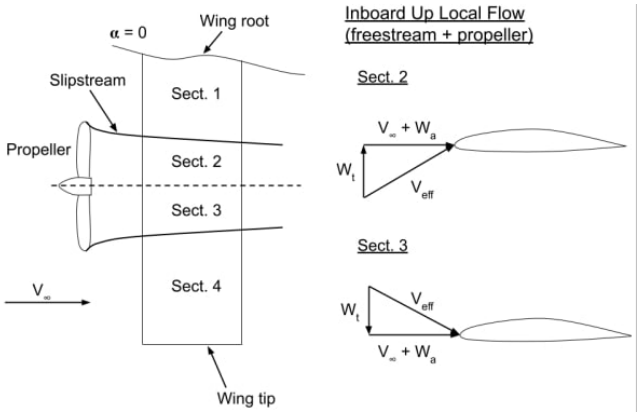

Figure 5: Diagram showing the affect of swirl on effective angle of attack on each half of a propeller wash

The data from the CFD report data used shows this phenomena in Fig.6 [6] by the asymmetry of the peaks in the ΔC_l distribution. Both side however still provide a positive change in lift coefficient. This implies that the increase due to the higher local velocity is a significantly greater affect than the affect of the change in angle of attack. This was also found in another CFD report as seen in appendix A.

As the effect of a higher local velocity appears to be the most impactful, it was decided to adapt the results from the CFD study according to this affect. As mentioned before the increase in lift

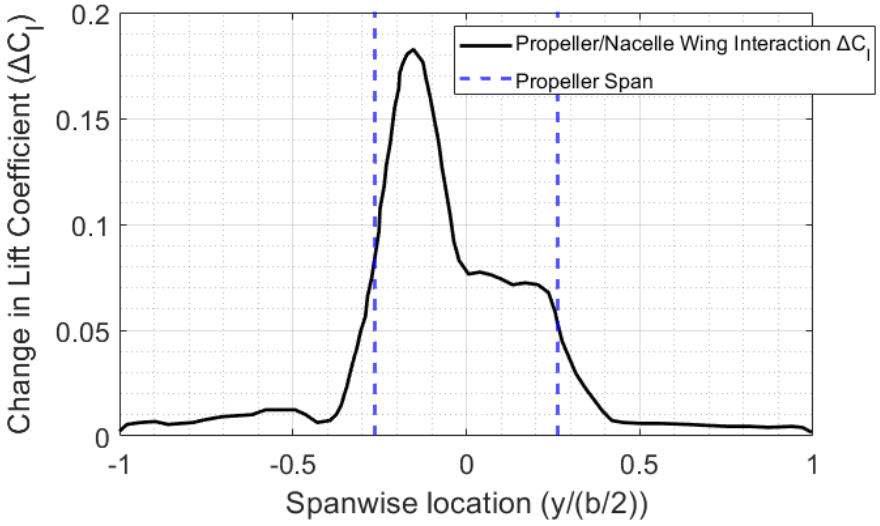

Figure 6: Scaled CFD ΔC_l results caused by Interaction between Propeller wash/nacelle and the wing.

due to this phenomena is described by equation 9 where lift is proportional to the propeller wash velocity squared. Equation 10 shows that that thrust produced by a propeller is proportional to the induced velocity squared (v_i) (assuming the induced velocity is of the same magnitude of the free stream velocity as is the case for the reference report [6]). As the propeller wash velocity is the sum of the induced and free stream velocity, this implies that the increase in lift caused by increased local velocity is proportional to the thrust produced by the propeller.

$$T = 2\rho A(U_\infty + v_i)v_i \qquad (10) \qquad C_T = \frac{T}{\frac{1}{2}q_\infty S} \qquad (11)$$

The change in lift coefficient data was therefore scaled proportional to the ratio of the report and this aircraft design's thrust coefficient as given by equation 11 to give the distribution given in fig.6. This aircraft's thrust coefficient, was calculated as half of the aircraft's total drag.

To incorporate this into the current lift distribution , the ΔC_l span-wise coordinates were translated to the correct propeller location and scaled based on the ratio of the reports and this design's propeller diameters. It was then superposed on top of the elliptical lift distribution previously optimized for. This gives the lift distribution accounting for the propeller wash/nacelle wing interaction shown in fig.7.

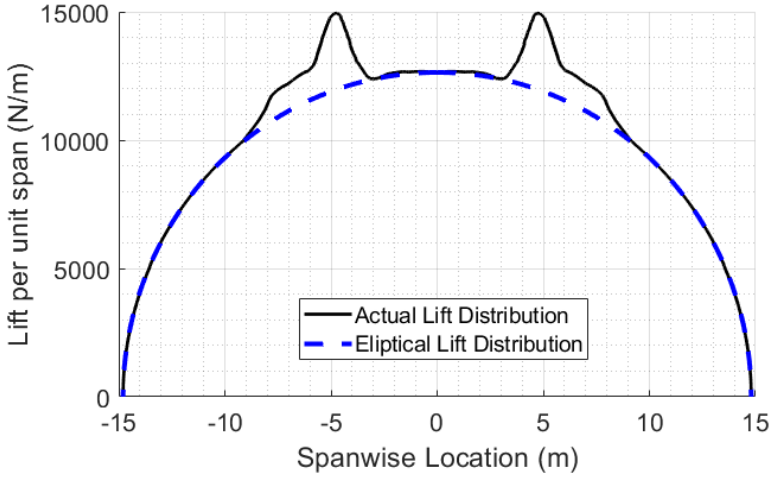

Figure 7: lift distribution after superposing the propeller/nacelle-wing ΔC_l distribution.

While this methodology makes many assumptions and uses data from a CFD with different variables and geometries, the results are similar in shape and magnitude to other results as can be seen in appendix A. Applying this crude method is also more accurate than simply ignoring it as this distribution is far from elliptical.

2.7 Aerodynamically Optimal Twist

The method used previously to optimize the lift distribution with twist was then used to enforce this higher fidelity lift distribution to be elliptical . This yielded the lift distribution seen in fig.8, with fig.9 showing the twist distribution required to enforce it. Once again, this method was able to near perfectly enforce an elliptical lift distribution. The twist distribution required is similar to the previous optimization but with variations to account for the peaks of the propeller wash ΔC_l distribution. This distribution successfully reduces the span-wise efficiency factor from 1.205 to 1.000 providing a large decrease in induced drag.

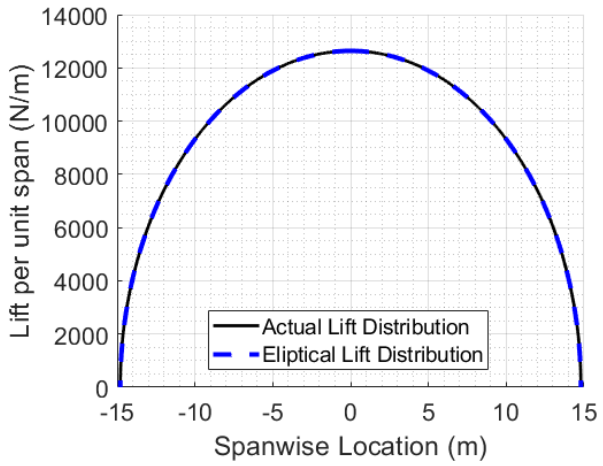

Figure 8: Lift distribution of aerodynamically optimized twist (without fuselage effects)

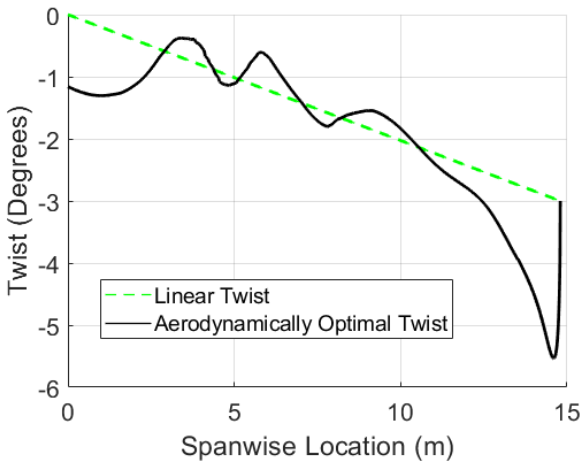

Figure 9: Aerodynamically optimized twist distribution

2.8 Wing Fuselage Interaction

Another component affecting the lift distribution is the fuselage. Over the width of the fuselage, the wing is not exposed to the free stream, reducing the lifting surface area and therefore lift. The addition of a faring also contributes to this affect.

The lift over the fuselage was modelled as a constant value and a discrete step to the otherwise elliptical lift distribution. The exact reduction in lift was determined by reducing the lift over the fuselage width until the wing span-wise efficiency factor ($1+\delta$) equaled a value of 1.15 from literature [9] for fuselage affects. This resulted in a decrease in total lift of 6.7%. To account for this the incidence angle was increased from 4.3° to 5.5° so that total lift again equalled the weight of the aircraft. This yielded the lift distribution seen in fig.10 where the distribution is elliptical except for the width of the fuselage.

The previous methodology of enforcing an elliptical lift distribution using twist was however not used over the width of the fuselage.This is due to the fact that wing is not exposed entirely to the free stream meaning it would not have the same lift curve slope. It is therefore not possible with the collocation method to accurately enforce the desired elliptical distribution. The final aerodynamically optimal twist is therefore taken as the twist seen previously in fig.9 which yields the the lift distribution seen in fig.10. Due to the way this distribution was determined, it's induced drag is 15% higher than an elliptical lift distribution due to the literature value of $1+\delta$=1.15 used to size the fuselage lift loss.

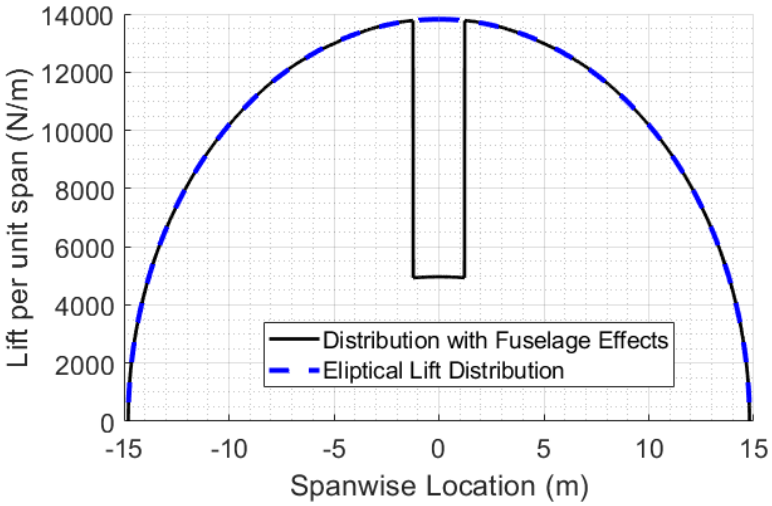

Figure 10: Aerodynamically optimized lift distribution after adding fuselage effects

2.9 Twist Smoothing

All the previous analysis yielded the optimal twist distribution from an aerodynamic perspective as seen in fig.9. This distribution is however constantly fluctuating, has sharp changes and is generally un-smooth. This is mainly due to the unusual shape of the ΔC_l caused by the propeller wash which the twist optimizes for. The twist distribution's gradient is also discontinuous due to the transcription of ΔC_l data consisting of discrete points. The prescribed twist of -3 at the end span also results in a sharp change in twist at the wing tip to avoid a discontinuity.

Such a un-smooth twist distribution could cause practical issues with manufacturing, control and potentially some aerodynamic downsides. To resolve this two strategies were employed. Firstly a set of qualitative requirements which a wing must adhere to were devised. Those conditions are as follows.

1. Over the entire span of an aileron, there must have a difference in twist of more than -3 degrees from the root to ensure the root stalls before tip.

2. Twist distribution over aileron span must be a gradual smooth distribution to provide feedback to pilot (Buffeting)

3. Local angle of attack should not exceed the linear region of lift curve slope or go below zero lift angle of attack. This is to stop sections of the wing stalling locally or producing negative lift respectively which would both increase drag.

In addition to these qualitative requirements, a strategy to quantify smoothness was found. Smoothness of a function can be quantified as the square of second derivative of a function. This informed the use of a smoothness index given by equation 12 [10] where a high index value represents poor smoothness. To quantify what a reasonable smoothness for an aircraft's twist distribution is, the twist distribution of a similar aircraft, the A380 was found shown in fig.11 [4]. The A380 is a conventional aircraft which is also significantly larger than this design meaning it likely has less restrictions on smoothness. The twist data available also has fairly few data points likely resulting in a more over-estimate of the smoothness index. The A380 does however have significantly thinner aerofoils with a 0.08 thickness to chord ratio compared to this design's thickness to chord ratio of 0.179. This combined with the lack of data available made this distribution the most appropriate to quantify reasonable smoothness.

$$I_s = (f''(x))^2 \tag{12}$$

The A380's twist distribution was normalized before the smoothness index was found as shown in fig.12. From this figure the smoothness index can be seen to be maximum at un-smooth sections where twist changes drastically. The maximum smoothness index value of 1.21E+05 was set as a maximum allowable smoothness parameter of this designs twist distribution. However to ensure the distribution doesn't have multiple of these un-smooth sections just under the maximum smoothness parameter, the integral of the A380s smoothness index was also found to be 3.41E+03 and set as the maximum smoothness index integral allowed.

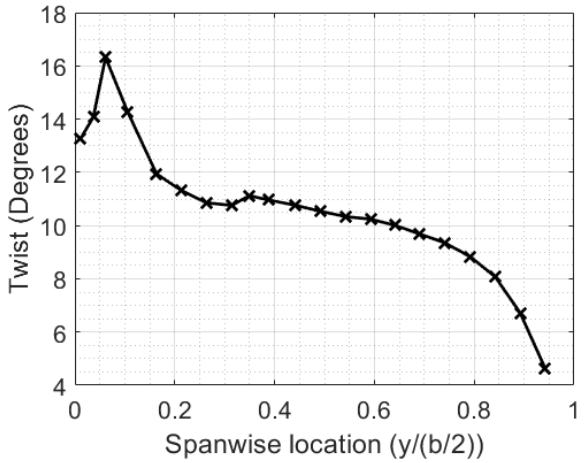

Figure 11: Span-wise Twist distribution of airbus A380

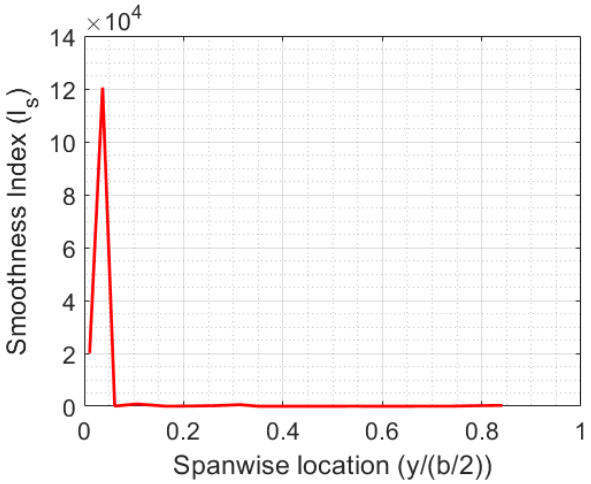

Figure 12: Smoothness index distribution of A380's twist distribution.

To produce a smooth a smoother twist distribution this design's aerodynamically perfect distribution was fitted with increasing order polynomials. For each order polynomial fit the maximum smoothness index as well as Integral smoothness index were recorded. These results can be seen in fig.13. From this figure it can be seen that as polynomial fit order increases (closer and closer fit of the un-smooth aerodynamically optimal twist), both the smoothness index and its integral increase exponentially.

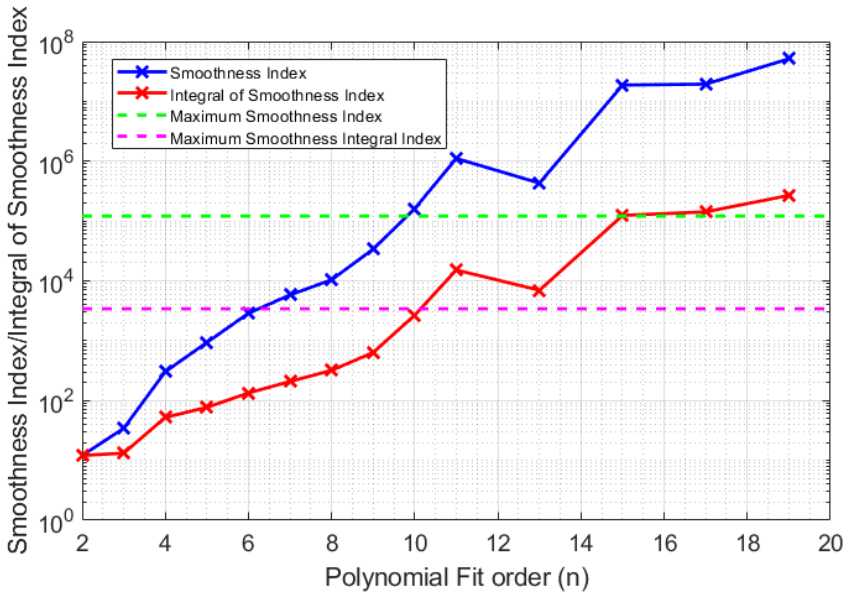

Figure 13: Semi-log graph of smoothness index and the integral of the smoothness index against polynomial fit order (n) when smoothing the aerodynamically optimized twist.

From this graph a polynomial of the ninth order can be seen to be the highest order fit still lower than both maximum index values. This therefore represents the highest order and therefore most optimal aerodynamic twist distribution which still meets the smoothness requirements. This ninth order fit can be seen in fig.14. This smoothed distribution follows the general trend of the optimal distribution but is far smoother. The maximum smoothness index has a value of 3.39E+04 as seen in fig15 while and its integral has a value of 6.35E+02 which are both significantly below the maximum allowable values of 1.21E+05 and 3.41E+03 respectively.

The highest un-smoothness for this ninth order fit occurs at the wing tips as seen in fig.15 which as previously mentioned could cause control-ability issues. However when comparing the smoothed distribution against the optimized distribution it can be seen to be far smoother and a fairly predictable stall characteristics. This smoothed fit is not forced to pass through the tip twist of -3°but the washout between the root and tip is however satisfied. This is because the tip has a twist angle of -5.21°and a root twist of -1.16°giving a washout of -4.05°. Finally the values of twist when added to the incidence of 5.5 are greater than the zero lift angle of attack α_0=-0.0609 and does not exceed the linear region of the lift curve slope at an angle of attack of 8 degrees [11]. As a ninth order polynomial fits all the quantitative and qualitative smoothness requirements, it was taken as the final twist distribution.

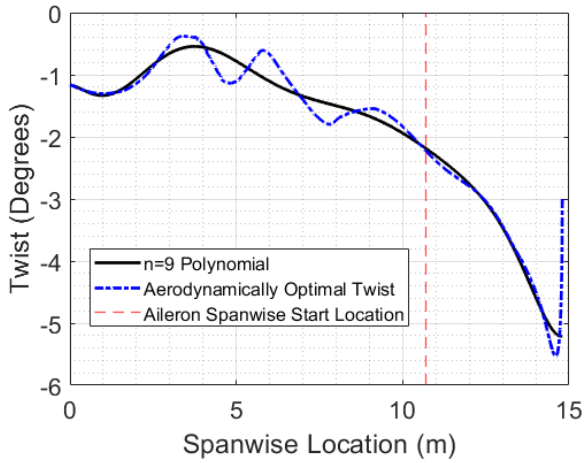

Figure 14: n=9 Order Smoothed Twist distribution vs aerodynamically optimal twist

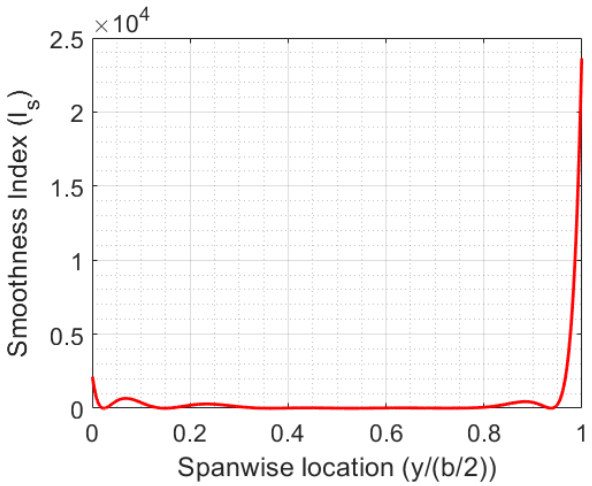

Figure 15: Smoothness index distribution of normalized n=9 order twist distribution.

Applying the smoothed twist distribution yields this design's final lift distribution seen in fig.16. Due to smoothing this distribution does not perfectly fit an elliptical distribution even outboard of the fuselage width. The largest deviation occurring in the region of the propeller wash as the twist distribution after smoothing is not able to change precisely enough to fully eliminate its affect on the lift distribution . This difference between the aerodynamically optimal twist and the smoothed twist distribution yielded a 2.65% increase in induced drag. Such a small increase in induced drag is a reasonable sacrifice in order to reduce the manufacturing cost , complexity and control issues which could be caused by the un-smoothed twist distribution. Smoothing of the twist distribution will also likely have better efficiency in off design conditions than the optimized distribution which may be over optimized.

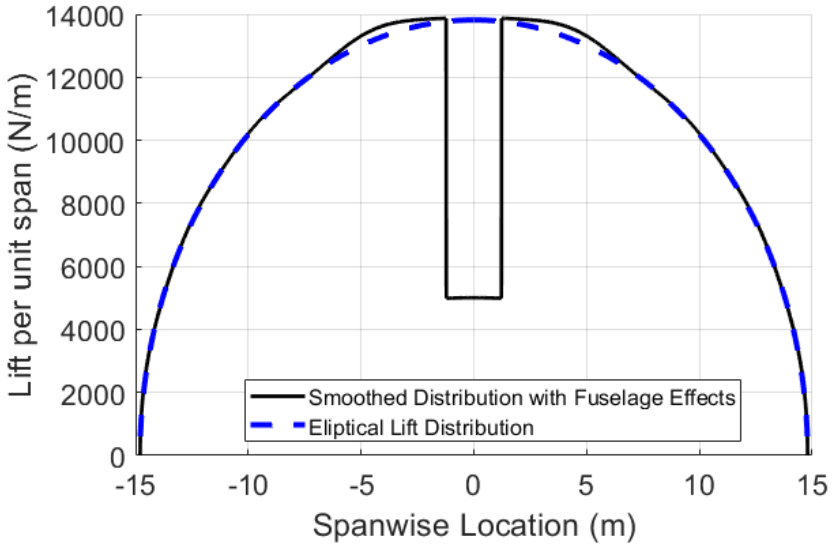

Figure 16: Final Lift distribution with 9th order smoothed twist distribution

2.10 Final Drag Analysis

The optimization of twist had many iteration resulting in different values of span-wise efficiency factor and therefore induced drag. A summary of these difference is given in table1. This table shows that the design lift distribution has a span-wise efficiency factor and therefore induced drag, 17.6% higher than a perfect elliptical lift distribution due to fuselage affects (15%) and smoothing (2.65%). This is a significant 19.6% improvement from the "worst case scenario" consisting of fuselage effects , propeller/nacelle interaction and linear twist. As the Oswald efficiency factor is the reciprocal of the span-wise efficiency factor, a value of $(1 + \delta)$=1.176 corresponds to a value of e=0.855. This is above the typical range for similar sized turboprop aircraft of 0.75-0.80 [12].

Lift Fistribution Distribution Iteration	Span-wise efficiency factor $(1+\delta)$
1.Constant Taper and Twist (fig.2)	1.017
2. Initial optimized twist (fig.3)	1.000
3. Un-optimized Propeller/Nacelle-Wing interaction (fig.7)	1.205
4. Aerodynamically optimized twist (fig.8)	1.000
5. Aerodynamically optimized twist with fuselage effect (fig.10)	1.150
6. Smoothed twist with fuselage effect (fig.16)	1.176
"Worst Case" Scenario	1.372
Reference Elliptical Lift Distribution	1.000

Table 1: Table summarizing span-wise efficiency factors for different lift distributions investigated

This value is a reasonable estimate as this design was able to optimize for just one design lift coefficient. Other aircraft must operate at multiple therefore cannot optimize their lift distributions for one condition as much. The improvement in aerodynamic efficiency of 19.6% over the "worst case" scenario and over similar aircraft is a significant improvement which is especially important for the novel ammonia design. This is because this reduction in drag reduces the thrust,fuel storage and fuel weight constraints which are all important for the viability of an ammonia powered aircraft.

Such a aerodynamic improvement could also allow for a reduction of the aircraft's aspect ratio in future design iterations which would lessen the aircraft's weight which is another design challenge of ammonia powered aircraft. This especially true as in future design iterations , the decrease in

efficiency caused by the fuselage could also be minimized by using either experimental or CFD tools to optimize twist over the fuselage.

The largest downside of the methodology used in this report is that it is over-optimized for one design lift coefficient. This would result in a decrease in aerodynamic benefits when operating at off design conditions. The smoothing of the twist distribution provides some improvement in this regard, but further investigation would hopefully yield aerodynamic improvements when operating at a range of operating conditions.

3 Fairing Design

3.1 Design

Most aircraft where efficiency is desirable have what is known as a wing-fuselage fairing. This is a purely aerodynamic structure which provides a smooth shape transition between the wing and the fuselage. Without a fairing the large increase in pressure which occurs around the wing's leading edge stagnation point causes separation of the nearby fuselage boundary layer [13]. Fairings also prevent separation caused by reversed flow at the trailing edge due to their shape [14]. Without a fairing, the interference factor between the wing and fuselage can increase from a value of 1 up to 1.4 [2]. This could result in an increase in zero lift drag from 0.0174 up to 0.0192 ($\Delta C_{D_{fair}}$=0.0018) for this design according to the component build up method conducted [15]. The extra volume inside the fairing can also be used for fuel storage which is especially important for this design as for safety reasons it was decided to store all ammonia in the wing.

Due to the complexity and 3D nature of the flow at the intersection of the wing and fuselage, typically extensive experimental or CFD analysis is required to find the exact optimal fairing shape. It was therefore decided to use an already existing standard fairing shape seen in fig.17 from literature as they previously have been shown to minimize drag caused by the aforementioned issues [16] .

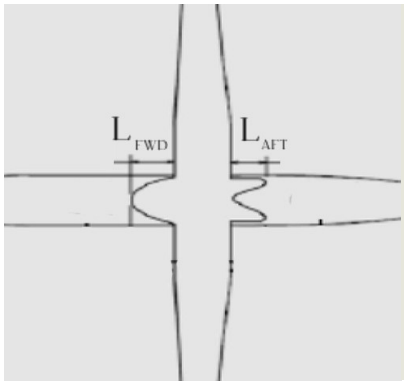

Figure 17: Standard fairing shape

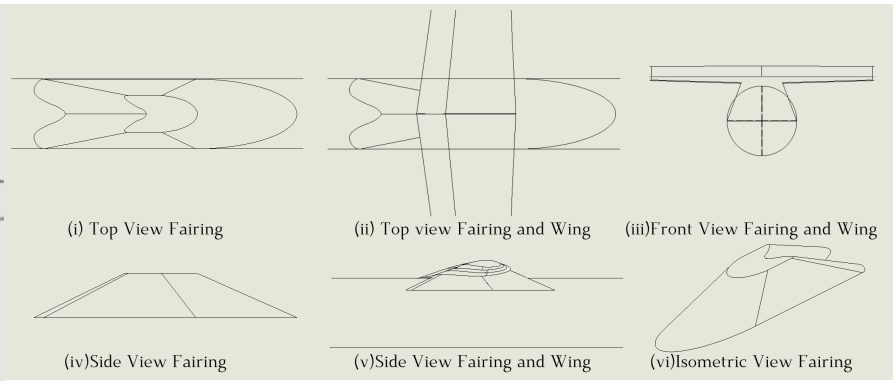

Figure 18: Various views of the designed fairing without and without the wing

This cross section is the base of the fairing situated at the centre-line of the fuselage. The width of the base is equal to the fuselage diameter while lengths L_{FWD} and L_{Aft} from fig.17 are suggested from literature to be 8% and 6% of the total fuselage length (L_f) respectively [16]. Finally the middle section length is equal to the root chord. Upon further research, CFD results for this same fairing shape were found for a high wing aircraft with similar fuselage length (30m) operating at a similar mach number (M=0.52). The CFD results from this report suggest drag is minimized when L_{FWD} and L_{Aft} are both increased to 12% of the the total fuselage length.This base cross section was then smoothly lofted to a truncated cross section seen in fig.18.i to the vertical height of leading edge of the wing root as can be seen in fig.18.v [17]. This however resulted in the fairing intersecting the wings trailing edge. The rear section was therefore shortened such that it was coincident with the trailing edge as seen in fig.18.v to prevent reversed flow. This reduced L_{Aft} to 8.27% of the fuselage length

which is still a reasonable length as it is still larger than the 6% suggested by literature . The final fairing design is therefore this loft with the intersecting volumes of the fuselage and wing removed.

3.2 Zero Lift Drag Calculations

While a fairing reduces drag resulting from interference of the wing and fuselage, the fairing itself will have an associated zero lift drag. To determine if a fairing would reduce overall drag, it is required to calculate if the benefit from decreasing the interference factor out ways the extra zero-lift drag. Due to the proximity of the fairing to the fuselage surface, the interaction of it with the boundary layer must also be considered.To do this a empirical methodology from ESDU data sheets summarized below was used with all calculations found in appendix.B .

This method initially involved determining the fairings geometric properties. Specifically its surface area and volume coefficients of C_S=0.17 and C_V=0.10 respectively were calculated using ESDU77028 [18]. This then allowed the calculation of the zero incidence profile drag from ESDU78019 [19] which yielded a value of $(C_D)_{\delta=0} = 0.00173$. This is an appropriate method as the wing incidence is set such that the fuselage and therefore the fairing will be parallel to the free stream .

This drag coefficient value is based on the assumption of being exposed to the free stream. However in the boundary layer, velocity decreases to zero with a power law profile therefore resulting in lower drag. The ESDU84035 method accounts for this difference with an effective dynamic pressure given by equation 13 [20] (for bodies are not entirely submerged with the boundary layer ($h/\delta > 1$)). In order to determine if this equation is appropriate, the height of the boundary layer was found empirically as a function of Reynolds number in order ensure it was smaller than the height of the fairing . This yielded a boundary layer height of 0.030m giving a value of $h/\delta = 19.4$ validating the use of equation 13. The variable m is the power law index for the variation of dynamic pressure across the boundary layer. Using equation 13 the ratio of effective to free stream dynamic pressure was found to be 0.97 implying the boundary layer has only a small 3% effect on drag. This yielded a final increase in form drag of $C_{D_{0,fair}}$=0.00168.

$$\frac{C_D}{(C_D)_{\delta=0}} = \frac{q_{eff}}{q_\infty} = (1 + \frac{\delta}{h}) + \frac{1}{1+m}\frac{\delta}{h} \tag{13}$$

This increase in drag is indeed less than the potential increase due to a change in interference factor ($\Delta C_{D_{fair}}$=0.0018), however it is only a small difference especially as the value for increased drag due to a higher interference factor is also based on a conservative estimate. The method for estimating the additional zero lift drag caused by the fairing is however likely a large over estimate because due to its unusual shape and intersections with other components, a large proportion of the fairing overlaps with the fuselage and wing meaning it does not interact with the free steam. Further investigation, likely either experimental or 3D CFD results are therefore needed to determine with certainty if a fairing yields an overall reduction in drag.

However due to the trend of similar aircraft, the extra volume the fairing provides for fuel storage as well as this initial drag calculation concluding a minor decrease in drag. It was chosen to install the designed fairing on the final design.

References

[1] Aircraft Design - an Open Educational Resource (OER) for Hamburg Open Online University (HOOU);. Accessed: 3.06.2023. https://www.fzt.haw-hamburg.de/pers/Scholz/HOOU/.

[2] Raymer D. Aircraft Design: A Conceptual Approach; 2018.

[3] Buxton O. Aerodynamics 3, AERO60001 Incompressible Flow PartIII. 2022.

[4] Airbus A380 Analysis;. Accessed: 5.06.2023. https://archive.aoe.vt.edu/mason/Mason_f/A380Roedts.pdf.

[5] Pusher vs. Puller Propeller Aircraft Compared;. Accessed: 8.06.2023. https://airplaneacademy.com/pusher-vs-puller-propeller-aircraft-compared/.

[6] Lars Mueller DKMJH Wolfgang Heinze. Aerodynamic Installation Effects of an Over-the-Wing Propeller on a High-Lift Configuration. 2014.

[7] van den Ende L. Swirl Recovery Vanes for Propeller Propulsion Systems. 2018.

[8] D'Angelo BK. Low-Order Modeling of Propeller-Wing Interaction Using a Modified Weissinger Method. 2021.

[9] AERODYNAMICS OF FINITE WINGS;. Accessed: 7.06.2023. https://eaglepubs.erau.edu/introductiontoaerospaceflightvehicles/chapter/finite-wing-characteristics/.

[10] The smoothest curve through a set of points;. Accessed: 3.06.2023. https://www.johndcook.com/blog/2009/02/06/the-smoothest-curve-through-a-set-of-points/.

[11] Ira Abbott LSJ Albert Doenhoff. Summary of Airfoil Data; 1945.

[12] Estimating the Oswald Factor from Basic Aircraft Geometrical Parameters;. Accessed: 17.06.2023. https://www.fzt.haw-hamburg.de/pers/Scholz/OPerA/OPerA_PUB_DLRK_12-09-10_Appendix_A_with_e_calc.pdf.

[13] C B Steenaert LMMB B W van Oudheusden. SIMPLIFIED DESIGN METHOD FOR A SYMMETRICAL WING-BODY FAIRING. 2002.

[14] Ney Rafael Secco GKJRRAM John Jasa. Component-based Geometry Manipulation for Aerodynamic Shape Optimization with Overset Meshes. 2018.

[15] Alsree HA. Ammonia-Powered regional Aircraft. 2023.

[16] Vecchia D. Aerodynamic guidelines in the design and optimization of new regional turboprop aircraft. 2014.

[17] Fabrizio Nicolosi DCVC Pierluigi Della Vecchia. Fuselage Aerodynamic Drag Prediction Method By CFD. 2015.

[18] Society RA. Drag of stub wings and fairings on a flat plate with a turbulent boundary layer at subsonic and supersonic speeds (ESDU 84035). 1984.

[19] Society RA. Geometrical characteristics of typical bodies (ESDU 77028). 1977.

[20] Society RA. Profile drag of axisymetric bodies at zero incidence for subcritical mach numbers (ESDU 78019). 1978.

Appendix

A Comparison of results to CFD report

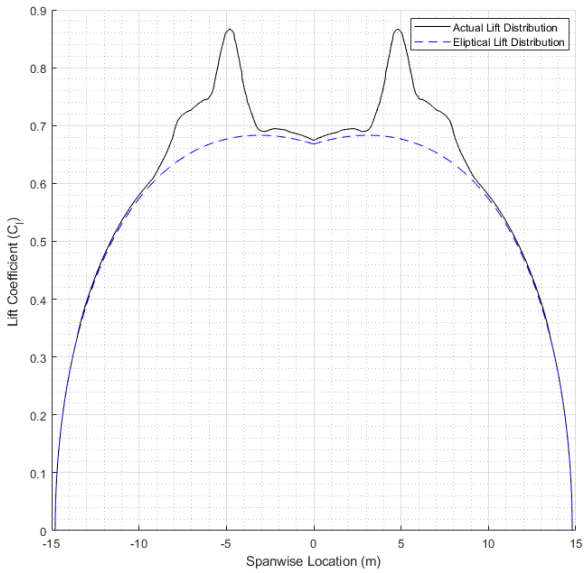

Figure 19: This report's results for Lift coefficient distribution

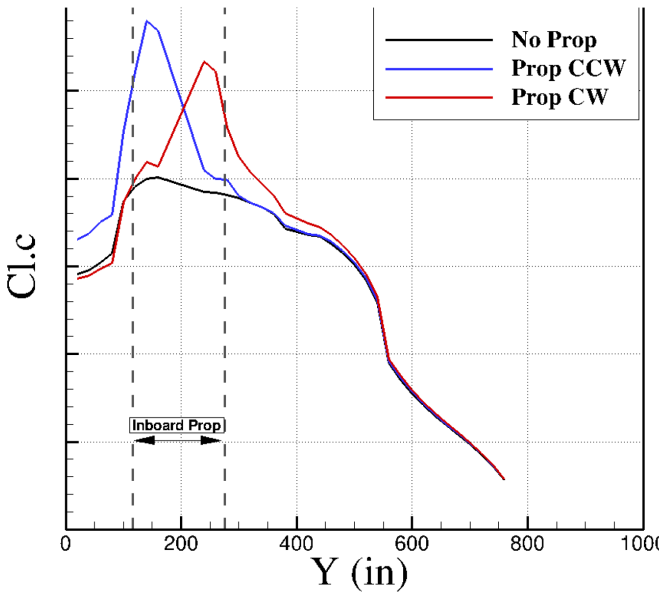

Figure 20: CFD results of Lift coefficient distribution

Both this design and the CFD report show similar shapes and magnitudes for the propeller wing interaction.

B Fairing Zero Lift drag calculations

Parameter	Value	Source
Surface Area Coefficient	0.165	ESDU77028
Volume Coefficient	0.096	ESDU77028
D/L	0.310	ESDU77028
n	0.680	ESDU78019
Ff	1.000	ESDU78019
Ff CS/Cvn̂	0.814	ESDU78019
lambda	1.305	ESDU78019
FM1	1.030	ESDU78019
FM2	0.950	ESDU78019
Fm2 Rl	77914396	ESDU78019
FM1 Cf0	0.00155	ESDU78019
Cf0	0.00150	ESDU78019
Cf/Cf0	0.880	ESDU78019
Cf	0.00132	ESDU78019
Cd (delta0)	0.00173	ESDU78019
m	1.000	ESDU84035
h/delta	19.4	ESDU84035
Cd/Cd(delta0)	0.974	ESDU84035
Cd	0.00168	ESDU84035